

Faraday waves in elongated superfluid fermionic clouds

P. Capuzzi^{1,*} and P. Vignolo^{2,†}

¹*Consejo Nacional de Investigaciones Científicas y Técnicas and Departamento de Física, FCEyN, Universidad de Buenos Aires, 1428 Buenos Aires, Argentina*

²*Institut Non Linéaire de Nice, Université de Nice-Sophia Antipolis, CNRS, 1361 route des Lucioles, 06560 Valbonne, France*

We use hydrodynamic equations to study the formation of Faraday waves in a superfluid Fermi gas at zero temperature confined in a strongly elongated cigar-shaped trap. First, we treat the role of the radial density profile in the limit of an infinite cylindrical geometry and analytically evaluate the wavelength of the Faraday pattern. The effect of the axial confinement is fully taken into account in the numerical solution of hydrodynamic equations and shows that the infinite cylinder geometry provides a very good description of the phenomena.

PACS numbers: 67.90.+z, 03.75.Ss, 05.45.-a, 47.54.-r

I. INTRODUCTION

The term Faraday waves refers to regular surface fringes which are excited by a vertical oscillatory motion in a nonlinear liquid [1]. The time-dependent spatially uniform driving leads *via* the nonlinear interaction between the wave excitations of the system to an instability towards the formation of spatial structure. Since the Faraday discovery, the phenomena of pattern formation and, more generally, of parametric amplification have been studied in diversified contexts, including convective fluids, nematic liquid crystals, nonlinear optics and biology [2]. Recently, Faraday waves have been experimentally created in a trapped atomic Bose-Einstein condensate (BEC) by a periodic modulation of the transverse confinement [3]. Nonlinearity in ultracold gases can be driven either by varying the scattering length, e.g., *via* Feshbach resonances, as proposed in this context by Staliunas *et al.* [4], or by varying the trap parameters as experimentally realized by Engels *et al.* [3]. Several phenomena connected to parametric amplification of excitations has been theoretically investigated in atomic BECs [5, 6, 7] and very recently, the properties of Faraday waves in confined BECs has been also explored [8, 9]. In all these cases, the periodic modulation of the nonlinearity leads to a parametric excitation of sound waves in the transverse direction respect to the modulation.

In this paper, we study the Faraday pattern formation in a superfluid Fermi gas in the BCS-BEC crossover at zero temperature. The physics of Faraday waves in a superfluid Fermi gas is richer than in an atomic Bose-Einstein condensate because the nonlinearity may also drive the microscopic features of the superfluid as described by its equation of state. This leads to strong variations in the pattern along the crossover.

We adopt the experimental conditions of Engels *et al.* [3] where the radial confinement of an elongated trap is

periodically modulated in time. By using a hydrodynamic description of the superfluid Fermi gas, we first treat the case of a infinite cylindrical gas to obtain an analytical expression for the spatial modulation of the Faraday pattern as a function of the driving frequency Ω , for small frequencies $\Omega \ll \omega_{\perp}$, ω_{\perp} being the transverse trap frequency. Then we numerically solve the three-dimensional hydrodynamic equations taking into account the axial confinement and investigate the formation of Faraday waves at higher frequencies ($\Omega \sim 2\omega_{\perp}$) where the fringes in the density profile can be experimentally visualized in cigar-shaped traps. Finally we compare the analytical prediction for the infinite cylinder with the numerical results and find that our analytical formula provides a good estimate of the pattern modulation even at $\Omega \sim 2\omega_{\perp}$.

The manuscript is organized as follows. Section II introduces the hydrodynamic description of the gas and derives the low frequency solution of the spatial pattern formation. In Sec. III we present the numerical results for the dynamics in a cigar-shaped trap and compare them with our analytical prediction. Section IV offers a summary and concluding remarks.

II. FARADAY EXCITATIONS IN A CYLINDER: HYDRODYNAMIC DESCRIPTION

Let us consider a superfluid Fermi gas at $T = 0$ confined by a cylindrical potential $V_{\perp}(\mathbf{r}) = m\omega_{\perp}^2 r^2/2$ with $r^2 = (x^2 + y^2)$ and m the atom mass. The dynamics of the density profile $n(\mathbf{r}, t)$ and the velocity field $\mathbf{v}(\mathbf{r}, t)$ is described by superfluid hydrodynamic equations, namely, the continuity equation

$$\partial_t n + \nabla \cdot (n\mathbf{v}) = 0 \quad (1)$$

and the Euler equation

$$m\partial_t \mathbf{v} + \nabla \left[\mu(n) + \frac{1}{2}m\omega_{\perp}^2 r^2 + \frac{1}{2}m\mathbf{v}^2 \right] = 0, \quad (2)$$

where $\mu(n)$ is the equation of state (EOS) of the gas which contains the microscopic details of the superfluid.

*Electronic address: capuzzi@df.uba.ar

†Electronic address: Patrizia.Vignolo@inln.cnrs.fr

A solution of the dynamics for a time-dependent ω_\perp can be obtained by relying on a scaling Ansatz. Following Ref. [10] we introduce the scaling parameter $b(t)$ and write

$$n(r, z, t) = \frac{1}{b(t)^2} n_0(r/b(t)) \quad \text{and} \quad \mathbf{v} = \frac{\dot{b}(t)}{b(t)} \mathbf{r}, \quad (3)$$

where $n_0(r)$ is the stationary solution of the Euler equation at $t = 0$, i.e., the Thomas-Fermi (TF) profile defined by $\mu(n_0(r)) = [\bar{\mu} - V_\perp(r)]$ with $\bar{\mu}$ the chemical potential. The scaling Ansatz in Eq. (3) satisfies the continuity equation for any form of $b(t)$ and is an exact solution of the Euler equation if the EOS follows a power law, $\mu(n) = \mathcal{C}n^\gamma$. In this case the scaling parameter obeys the differential equation

$$\ddot{b} + \omega_\perp^2(t) b - \frac{\omega_\perp^2}{b^{2\gamma+1}} = 0. \quad (4)$$

Notice that if the EOS is not a power law, one can still introduce an effective exponent $\bar{\gamma}$ and exploit the same procedure [12] to find an approximate solution of the dynamics.

To excite Faraday waves, we modulate the transverse trap frequency as

$$\omega_\perp(t) = \omega_\perp(1 + \varepsilon \sin \Omega t) \quad (5)$$

where Ω is the driving frequency and ε is a small parameter, $\varepsilon \ll 1$. For $\Omega \ll \omega_\perp$, Eq. (4) has the solution [11]

$$b(t) \simeq 1 - \alpha \sin(\Omega t) \quad (6)$$

with $\alpha = \varepsilon/(\gamma + 1 - \Omega/(2\omega_\perp)) \simeq \varepsilon/(\gamma + 1)$ in agreement with the expression found in Ref. [8] for an ultracold Bose gas ($\gamma = 1$). For larger Ω , the solution of Eq. (4) represents a forced breathing mode which does not adiabatically follow the forcing frequency. For instance, when the driving frequency is close to the natural breathing mode $\Omega = \sqrt{2\gamma + 2}\omega_\perp$, the system exhibits the resonant solution

$$b(t) \simeq 1 + \frac{\varepsilon \omega_\perp t}{\sqrt{2 + 2\gamma}} \cos(\Omega t) \quad (7)$$

valid for small t . For larger t , the resonant solution can be seen to exponentially increase.

A. Excited states

The modulation of the nonlinearity excites sound-like phonons in the z -direction which, in turn, lead to the instability of the scaling solution (3). These excited states breaking the axial symmetry can be investigated by a linear analysis, i.e., by setting $n(r, z, t) = n_0(r/b)/b^2 + \delta n(r, z, t)$ and linearizing Eqs. (1) and (2) in δn we arrive the following equation

$$m \partial_t^2 \delta n = \frac{1}{b^{2\gamma}} \nabla \cdot \left[n_0 \left(\frac{r}{b} \right) \nabla \left(\frac{\partial \mu}{\partial n} \Big|_{n=n_0(\frac{r}{b})} \delta n \right) \right], \quad (8)$$

that is valid for small velocity fields, i.e., $\Omega \ll \omega_\perp$. Equation (8) is a sound-wave equation for the instantaneous density. Using the solution Eq. (6) and developing to first order in α , Eq. (8) gives rise to

$$m \partial_t^2 \delta n = \nabla \cdot \left[n_0|_{\alpha=0} \nabla \left(\frac{\partial \mu}{\partial n} \Big|_{\alpha=0} \delta n \right) \right] + 2\alpha \sin(\Omega t) \mathcal{F}(n_0|_{\alpha=0}, \mu(n)|_{\alpha=0}, \delta n) \quad (9)$$

with

$$\mathcal{F} = \nabla \cdot \left[\gamma n_0 \nabla \left(\frac{\partial \mu}{\partial n} \delta n \right) - \frac{r^2}{R_\perp^2} \frac{\partial n}{\partial \mu} \nabla \left(\frac{\partial \mu}{\partial n} \delta n \right) - n_0 \nabla \left(\frac{r^2}{R_\perp^2} \frac{\partial n}{\partial \mu} \frac{\partial^2 \mu}{\partial n^2} \delta n \right) \right]_{\alpha=0}. \quad (10)$$

where $R_\perp = \sqrt{2\bar{\mu}/m\omega_\perp^2}$ is the TF radius of the gas. The right-most term in Eq. (9) proportional to $\sin(\Omega t)$ behaves like a source for excitations in the linear response regime. Expressing δn in its Fourier components, $\delta n = \sum_j \delta n_j(r, z) \cos(\omega_j t + \phi_j)$, one can easily demonstrate that the lowest-frequency Fourier component that is resonant with the perturbation corresponds to $\omega_0 = \Omega/2$. This is a general result for dynamical systems governed by Mathieu-type equations [13] as Eq. (9). We keep only the resonant term in Eq. (9) and make the Ansatz $\delta n_0(r, z) = \delta n_0(r) \cos(qz)$, corresponding to counter propagating axial phonons with momenta $\pm q$. To find an estimate of q , we assume that Ω is small enough to consider only the sound mode δn_0 and therefore take $\delta n_0(r) = (\partial \mu / \partial n)^{-1}$ evaluated at $\alpha = 0$, i.e., the sound limit solution for $q \rightarrow 0$ and $\Omega \rightarrow 0$ at $t = 0$ (see Ref. [14]). By integrating in the radial plane one obtains

$$m \left(\frac{\Omega}{2} \right)^2 \int \left(\frac{\partial \mu}{\partial n} \Big|_{\alpha=0} \right)^{-1} d^2 r = q^2 \int n_0|_{\alpha=0} d^2 r + O(\alpha^2) q^2 \quad (11)$$

which, for a power-law EOS leads to

$$q = \frac{\Omega}{2} \sqrt{\frac{m(\gamma + 1)}{\gamma \bar{\mu}}}, \quad (12)$$

neglecting second-order terms in α . The above expression can be directly linked to the sound velocity c_s [14] in an elongated superfluid by $q = \Omega/(2c_s)$.

By introducing the wavelength of the Faraday pattern $d = 2\pi/q$ it is possible to evaluate the number of fringes \mathcal{N} in an elongated superfluid confined by an harmonic potential $V_{\text{ext}}(r, z) = V_\perp(r) + m\omega_z^2 z^2/2$. Given that the axial extent of the density can be written as $L_z = 2R_\perp/\lambda$ where $\lambda = \omega_z/\omega_\perp$ and neglecting edge effects, Eq. (12) yields

$$\mathcal{N} = \frac{L_z}{d} = \frac{1}{\pi \lambda} \sqrt{\frac{\gamma + 1}{2\gamma}} \frac{\Omega}{\omega_\perp}. \quad (13)$$

For $\gamma = 1$, \mathcal{N} is in good agreement with the experimental data of Engels and coworkers [3] even for large

ε and Ω , where the procedure we used to derive it is not fully justified. Equation (13) predicts that the number of Faraday fringes varies by a factor of $2/\sqrt{5}$ in the BCS-BEC crossover and thus it could be easily observed in current experimental setups with strongly elongated traps [15, 16], as discussed in the following section.

III. NUMERICAL RESULTS

The numerical solution of the superfluid hydrodynamic equations allows to fully take into account the role of the axial confinement and to get over the approximation of small frequencies. To compute the dynamics we first map the superfluid density $n(\mathbf{r}, t)$ and velocity field $\mathbf{v}(\mathbf{r}, t)$ to the complex field $\psi(\mathbf{r}, t) = \sqrt{n} e^{iS}$, with $\mathbf{v} = \hbar \nabla S / m$. In this way the dynamical equations can be cast in a Gross-Pitaevskii-like equation of motion for ψ . We then discretize this equation in the (r, z) plane and solve it using a 5th-order Runge-Kutta method [17]. A mesh of 200×400 points in the (r, z) plane and a time step $dt = 10^{-4}/\omega_{\perp}$ are usually enough to compute the evolution until $t = 500/\omega_{\perp}$.

We consider a Fermi gas with $N = 5 \times 10^5$ ^{40}K atoms trapped in a cylindrically symmetric trap with $\omega_{\perp} = 160.5 \text{ Hz}$ and $\omega_z = 7 \text{ Hz}$, and fix the modulation parameter $\varepsilon = 0.05$. The superfluid is described by the EOS developed by Hu *et al.* [18] and parametrized in terms of $1/(k_F a)$ where k_F is the Fermi wavevector $k_F = (3\pi^2 n)^{1/3}$ and a is the s -wave scattering length. If not differently specified, in the following we refer to a continuous modulation of the transverse trap frequency at $\Omega = 2\omega_{\perp}$.

From the numerical solution of the density profile $n(r, z, t)$ we have computed the axial and radial RMS widths, and the column densities $n_{1D}(z, t) = \int dy n(x=0, y, z, t)$. These are shown in Figs. 1-3 together with their Fourier transforms for the case of the Fermi gas in the BCS regime ($a/a_0 = -10^{-1}$, a_0 being the Bohr radius). The dynamics of the width Δr (Fig. 1) is dictated by the driving frequency coupled to the transverse breathing mode, which for the gas in the BCS limit is $\omega = \sqrt{10/3}\omega_{\perp}$. This reflects the competition between the forcing and the natural breathing mode. Furthermore, within the scaling approach of Sec. II, the axial width evolves in time with $b(t)$, i.e., $\Delta r(t) = \Delta r(0) b(t)$. Indeed, the numerical solution of the ordinary differential equation (4) reproduces very well the behavior of Δr for the axially confined gas before the Faraday instability sets in. As noted earlier, we would like to emphasize that due to the vicinity of the natural breathing mode and the driving frequency, Δr does not simply adiabatically follows ω_{\perp} as clearly shown in the figure.

The time evolution of the axial width Δz and its Fourier transform are instead illustrated in Fig. 2. Similarly to the radial width, the evolution of Δz is dominated by the forcing frequency Ω and the axial breathing mode, that is $\sqrt{12/5}\omega_{\perp}$ in the BCS case. The excita-

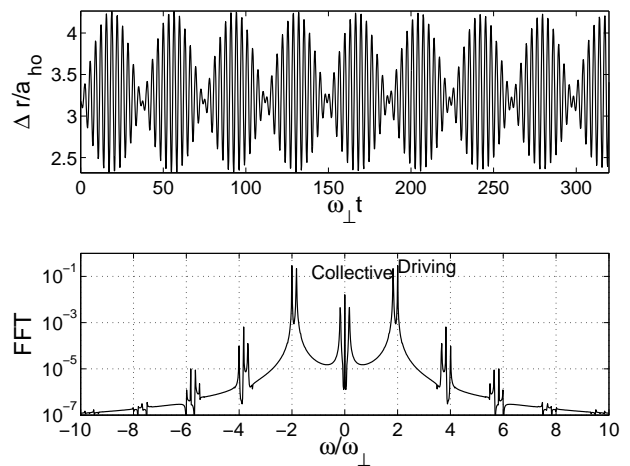


FIG. 1: Time evolution of the transverse width Δr for a Fermi superfluid in the BCS limit (see text). The top panel depicts Δr (in units of $a_{ho} = \sqrt{\hbar/(m\omega_{\perp})}$) as a function of t (in units of ω_{\perp}^{-1}) and the bottom panel depicts its Fourier transform (in arbitrary units and logscale) as function of ω/ω_{\perp} .

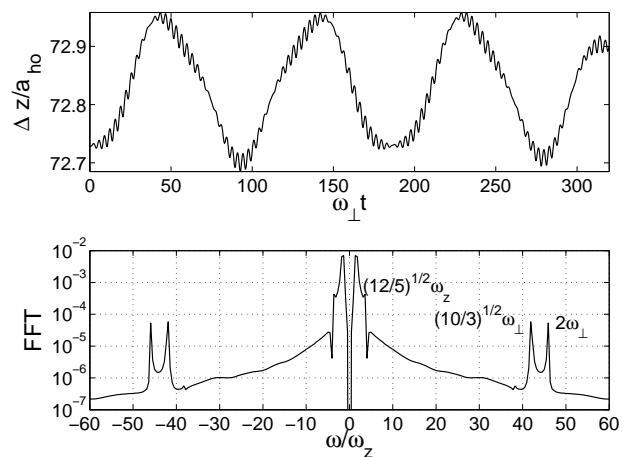


FIG. 2: Idem Fig. 1 for the axial width Δz . The Fourier transform in the bottom panel is displayed in arbitrary units and logscale, and the frequency ω in units of ω_z .

tion of the axial breathing mode is a consequence of the coupling of the radial and axial directions imposed by the three-dimensional trap and should not be expected in the infinitely long cylinder discussed in Sec. II.

Although Δr and Δz show no evidence of the frequency $\Omega/2$ in their spectra, the column density at the center of the trap (Fig. 3) clearly exhibits it. The relative importance of this frequency in the spectrum of n_{1D} is accentuated with time as a result of the formation of the Faraday wave, this effect can be seen by analyzing the Fourier transform for different time intervals.

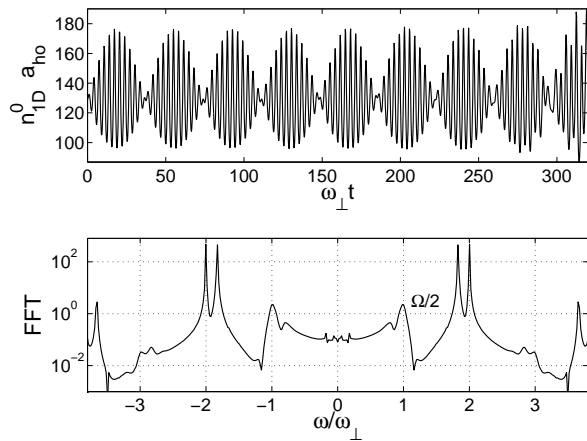


FIG. 3: Time evolution of the column density at the trap center $n_{1D}^0 = n_{1D}(z=0)$. The top panel shows n_{1D}^0 (in units of a_{ho}^{-1}) as a function of time t (in units of ω_{\perp}). The bottom panel displays its temporal Fourier transform (in arbitrary units and logscale) as function of ω/ω_{\perp} .

A. Onset of Faraday wave formation

The Faraday instability becomes visible when the momentum distribution develops components at the momenta $\pm q$ corresponding to pairs of counter-propagating axial excitations of frequency $\Omega/2$. In Fig. 4 we display the formation of a Faraday wave in the density profile of a gas in the weakly BCS limit with $a = -10^{-1}a_0$. After approximately 50 driving periods, the appearance of transverse fringes along the axis of the cigar is clear and we can say that the Faraday instability has been fully set in. For longer times, as the Faraday waves increase their amplitude, a large number of modes interacts and the Faraday pattern develops several complicated spatial and temporal structures, resembling those of spatio-temporal chaos as expected in confined hydrodynamic flows [2]. This regime cannot be accounted for by the simplified analysis of Sec. II and requires a more demanding numerical effort.

The onset time of the Faraday waves varies through the BCS-BEC crossover. The growth rate of the spatial pattern can be evaluated by computing the fraction

$$\delta_N(t) = \left(\frac{\int \delta \tilde{n}^2(z, t) dz}{\int \tilde{n}_0^2(z, t) dz} \right)^{1/2} \quad (14)$$

where $\tilde{n}_0(z, t)$ is the scaled density extracted from the numerical solution by fitting a TF profile $n(z) = \mathcal{A}(\tilde{\mu} - m\omega_z^2 z^2/2)^\eta$ to the integrated density $n_{1D}(z, t)$ at each time t , and $\delta \tilde{n} = n_{1D}(z, t) - \tilde{n}_0(z, t)$. The magnitude δ_N represents the normalized deviation of the density respect to the scaling solution and can therefore be related to the amplitude of the Faraday wave. The evolution of δ_N is illustrated in Fig. 5 for three values of a in the BCS, unitarity and BEC regimes. In the BCS and in the unitarity limits the growth rates are comparable as

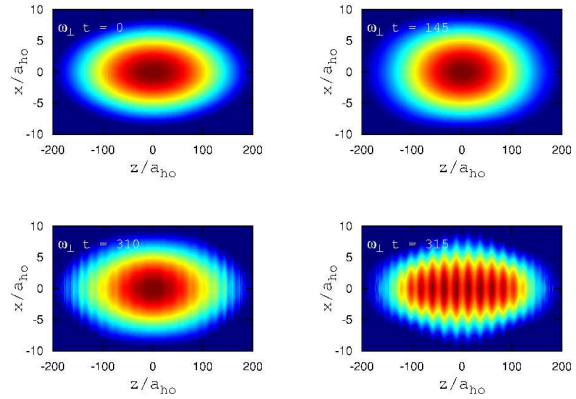


FIG. 4: (color online) Density plots $n(x, y=0, z, t)$ of a Fermi gas in the BCS regime at several times t during the transverse frequency modulation.

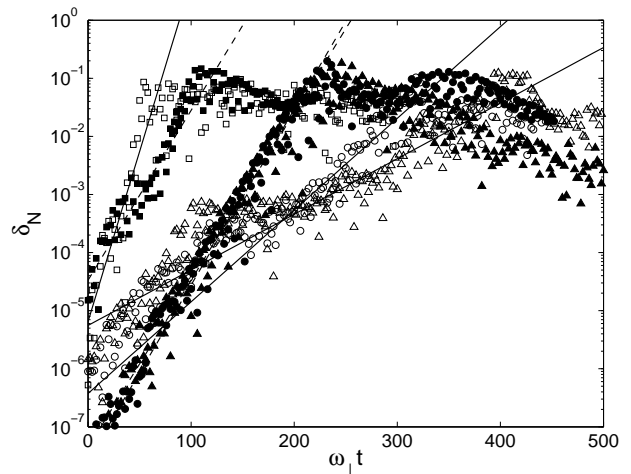


FIG. 5: Fraction δ_N (in logscale) as a function of the time t (in units of ω_{\perp}^{-1}) for $a/a_0 = -10^{-1}$ (circles), -10^5 (triangles), and 10^3 (squares). The empty symbols corresponds to the continuous driving while the full ones to the 3-cycle driving. The lines are guides to eyes for better visualizing the growth rates.

the excitation spectra in both regimes are the same. In the BEC limit, instead, the onset is more rapid since the driving frequency $\Omega = 2\omega_{\perp}$ corresponds to a collective mode of the cloud.

Faraday waves can be also created by driving the transverse confinement for only few cycles [3]. However, in this case, the growth rate of the pattern is modified. For instance, we have found that for a 3-cycle perturbation, the rate for a BCS and a unitarity superfluid Fermi gas increases approximately by a factor of 2–3, while in the BEC limit it decreases by a factor of 1.5 approximately. For our choice of Ω , the driving frequency and the breathing modes are in competition in the BCS and unitarity limits and the continuous excitation may delay the formation of the pattern. In the BEC limit, $\Omega = 2\omega_{\perp}$ corre-

sponds to the breathing mode and the onset of the instability is more rapid by continuously exciting the system at resonance. Note that the total growth time of a Faraday wave may also depend on the numerical noise caused by the discrete space-time grids, but the growth rates in the linear regime should not be modified.

B. Faraday wavevector through the crossover

A further observable which depends on the crossover is the wavevector q of the Faraday pattern, as already outlined in Sec. II. Experimentally, q can be deduced by measuring the interfringe distance d at the center of the cloud. The interfringes obtained in the numerical simulation can be observed in Fig. 6 where the integrated density n_{1D} has been plotted together with the topview density plots for $a/a_0 = -10^{-1}$, -10^5 , and 120 corresponding to the BCS, unitarity and BEC regimes, respectively. It is worth stressing that at $a = 120a_0$, the transverse size displays an impact-oscillator behavior as observed for an atomic BEC at the breathing frequency [3, 9]. The resulting strong modulation of the nonlinearity speeds up formation of the Faraday waves and impose severe numerical limitations.

Through the crossover, from the BCS to the BEC limits, at fixed number of fermions, both the size of the cloud and the interfringe d decrease since they are both proportional to $\sqrt{\mu}$; however, d decreases less rapidly because of the factor $\sqrt{\gamma/(1+\gamma)}$ with a corresponding slight modification of the fringe number. As a result in the BCS and unitary regimes the number of fringes are the same as can be seen in Fig. 6, i.e., 16 for $a = -0.1a_0$ and -10^5a_0 , while in the BEC regime ($a = 120a_0$), the number of fringes diminishes by a factor of $2/\sqrt{5}$, corresponding to 14 fringes approximately. In more elongated traps as that used in the ENS experiments [16] with $\lambda \simeq 0.18$, the variation of \mathcal{N} through the crossover can be more important, from $\mathcal{N} = 41$ in the BCS limit to $\mathcal{N} = 37$ in the BEC limit at $\Omega = 2\omega_{\perp}$.

In Fig. 7 we compare the Faraday wavevector $q = 2\pi/d$ as observed in the numerical simulation with that predicted for a soundlike excitation at $\Omega/\omega_{\perp} = 2$ and 1.5. Mimicking a real experiment, d has been measured at the center of the density profile and the error bars have been evaluated from its variance during several time steps. Equation (11) instead has been evaluated by using the EOS deduced by Hu and coworkers [18]. The results show that Eq. (11) provides a good estimate of the function $q(\Omega)$ through all the crossover in particular for $\Omega = 2\omega_{\perp}$. On the other hand, for $\Omega = 1.5\omega_{\perp}$ the numerical result for $a = 10^3a_0$ lies well above the prediction. Indeed, by analyzing the FFT of n_{1D}^0 in this case, we found that the transverse modulation at $\Omega = 1.5\omega_{\perp}$ also excites the collective mode of the BEC at $\Omega = 2\omega_{\perp}$ similarly to what was found experimentally in Ref. [3]. As a consequence, the mode at $\Omega = 2\omega_{\perp}$ dominates the generation of longitudinal excitations even when modulating at $\Omega = 1.5\omega_{\perp}$

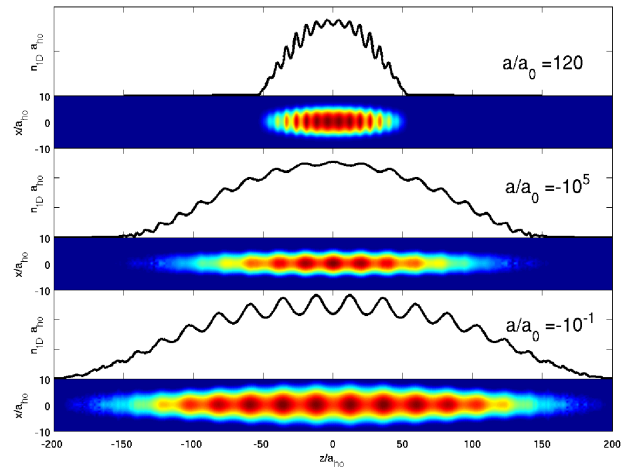


FIG. 6: (color online) Density plots and integrated density n_{1D} as function of position (in units of a_{ho}) after the Faraday instability has been set in. Top, middle, and bottom panels correspond to $a/a_0 = 120$, -10^5 , and -10^{-1} , respectively.

and thus the numerical result should be compared with the prediction at $\Omega = 2\omega_{\perp}$, as shown by a cross in Fig. 7. For comparison, we have also evaluated the Faraday wavevector predicted by Eq. (11) using the mean-field BCS EOS, $\mu(n) = \hbar^2 k_F^2 / 2m (1 + \frac{4}{3\pi} k_F a)$. It is worthwhile remembering that this EOS predicts the collapse of the fermionic mixture for strong attractive interactions, as indicated by the divergence of q shown in dashed line in Fig. 7.

IV. SUMMARY AND CONCLUDING REMARKS

In summary we have studied the formation of Faraday patterns in an elongated superfluid Fermi gas in the BCS-BEC crossover. We simulated an experiment where nonlinearity is driven by modulating the transverse confinement and compared the numerical results with an analytical estimate derived neglecting the axial confinement and for low frequencies. The peculiarity of a superfluid Fermi gas respect to an atomic Bose-Einstein condensate is that the nonlinear term controls the microscopic features of the superfluidity and that the pattern modulation depends on the crossover itself. Moreover the pattern growth rate varies through the crossover as a consequence of the different spectra. Our numerical and analytical predictions may be observed in current experiments with superfluid Fermi gas in strongly elongated traps [15, 16].

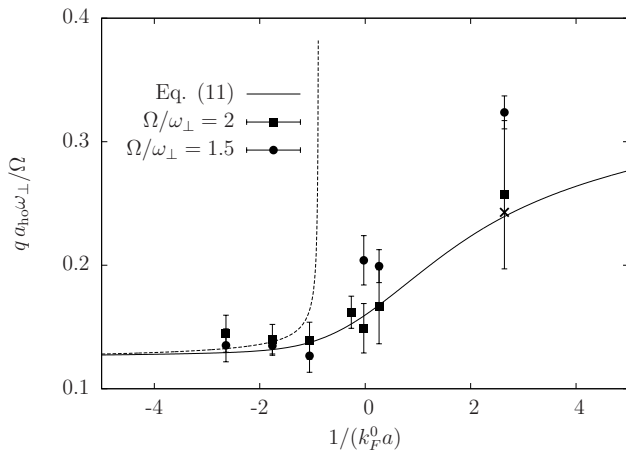


FIG. 7: Comparison of the ratio q/Ω between the observed Faraday wavevector q (in units of a_{ho}) and the driving frequency Ω (in units of ω_{\perp}) with that predicted for a soundlike excitation (Eq. (11)) as functions of $1/(k_F^0 a)$, where k_F^0 is the Fermi momentum of the noninteracting gas at the trap center. The error bars have been estimated from the variance of d during several time steps. The cross corresponds to a result obtained by modulating at $\Omega/\omega_{\perp} = 1.5$ corrected by taking into account the induced excitation at $\Omega = 2\omega_{\perp}$ (see text). The dashed line corresponds to the prediction of Eq.(11) with the BCS mean-field EOS.

Acknowledgments

This work was partially supported by grants PICT 31980/05 from ANPCyT and PIP 5138/05 from CONICET, Argentina. P.C. wishes to acknowledge the kind hospitality of the INLN where most of this work was performed.

-
- [1] M. Faraday, Phil. Trans. R. Soc. London **121**, 299 (1831).
[2] For a general review, see M.C. Cross and P.C. Hohenberg, Rev. Mod. Phys. **65**, 851 (1993).
[3] P. Engels, C. Atherton, M.A. Hoefer, Phys. Rev. Lett. **98**, 095301 (2007).
[4] K. Staliunas, S. Longhi, and G. J. de Valcarcel, Phys. Rev. Lett. **89**, 210406 (2002).
[5] J. J. García-Ripoll, V. M. Pérez-García, and P. Torres, Phys. Rev. Lett. **83**, 1715 (1999).
[6] C. Tozzo, M. Krämer, and F. Dalfovo, Phys. Rev. A **72**, 023613 (2005).
[7] M. Modugno, C. Tozzo, and F. Dalfovo, Phys. Rev. A **74**, 061601(R) (2006).
[8] Yu. Kagan, L.A. Manakova, Phys. Lett. A **361**, 401 (2007).
[9] A.I. Nicolin, R. Carretero-Gonzalez, and P.G. Kevrekidis, Phys. Rev. A **76**, 063609 (2007).
[10] Yu. Kagan, E.L. Surkov, and G.V. Shlyapnikov, Phys. Rev. A **54**, R1753 (1996).
[11] Yu. Kagan, L.A. Manakova, Phys. Rev. A **76**, 023601 (2007).
[12] H. Hu, A. Minguzzi, X.-J. Liu, M. P. Tosi, Phys. Rev. Lett. **93**, 190403 (2004).
[13] For a brief discussion on Mathieu and Hill equations on the context of nonlinear Schrödinger equations see Ref.[5] and references therein.
[14] P. Capuzzi, P. Vignolo, F. Federici, and M.P. Tosi, Phys. Rev. A **73**, 021603(R) (2006).
[15] J. Joseph, B. Clancy, L. Luo, J. Kinast, A. Turlapov, and J. E. Thomas, Phys. Rev. Lett. **98**, 170401 (2007).
[16] L. Tarruell, M. Teichmann, J. McKeever, T. Bourdel, J. Cubizolles, L. Khaykovich, J. Zhang, N. Navon, F. Chevy, C. Salomon, Proceedings of the International School of Physics *Enrico Fermi*, Course CLXIV, Varenna, 20 - 30 June 2006, edited by M. Inguscio, W. Ketterle, and C. Salomon.
[17] W.H.Press, S. A.Teukolsky, W. T. Vetterling, and B. P. Flannery, *Numerical Recipes in Fortran 77: The Art of Scientific Computing*, 1992, Cambridge University Press.
[18] H. Hu, X.-J Liu, and P.D. Drummond, Europhys. Lett. **74**, 574 (2006).